

Supersolid phase in fully frustrated Josephson junction arrays

Luigi Amico, Giuseppe Falci, Rosario Fazio and Gaetano Giaquinta

Istituto di Fisica, Facoltà di Ingegneria, Università di Catania, viale A. Doria 6, I-95129

Catania, Italy

Abstract

We study the phase diagram and the excitation spectra of an array of small Josephson junctions at $f = 1/2$ and arbitrary charge frustration. We find that the supersolid region in the phase diagram is larger than the correspondent region at $f = 0$ and it includes two different phases. In the chiral supersolid (SS) charges and vortices are arranged in a checkerboard pattern on a 2×2 supercell analogously to the unfrustrated case. We find a new phase, which we term *non-chiral supersolid* (NCSS), which has no corresponding phase at $f = 0$. The excitation spectra in the supersolid regions show particle like dispersions which is related to the defectons. The defecton condensation leads to superfluidity in the presence of charge ordered background.

arXiv:cond-mat/9608044v1 8 Aug 1996

I. INTRODUCTION

Josephson Junctions Arrays (JJA) are ideal model systems to study a variety of phase transitions induced by thermal or quantum fluctuations [1,2]. These latter play a major role if the superconducting islands are of submicron size and drive the zero temperature Superconductor–Insulator (SI) phase transition. The two characteristic energy scales in the system are the Josephson energy J which is associated to the tunneling of Cooper pairs between neighboring islands and the charging energy U which is the energy cost to add an extra Cooper pair on a neutral island. The electrostatic energy tends to inhibit the Josephson tunneling: indeed a finite U produces quantum fluctuations of the phases ϕ 's of the superconducting order parameter $\Delta e^{i\phi_i}$ one each island. If $J \gg U$ the system is superconducting since the fluctuations of the ϕ 's are small and the system is globally coherent. In the limiting case $J/U \rightarrow \infty$, which will be referred as the *classical* case, the electrostatic energy plays no role. In the opposite limit, $J \ll U$, the array is a Mott insulator since strong quantum fluctuations of ϕ_i prevent the system to reach coherence (Coulomb blockade of Cooper pairs). The SI phase transition in JJA has been studied in great detail both experimentally [3] and theoretically [4]. The effect of disorder and the presence of an additional glass transition has been studied in Ref. [5]. At the transition the system could be a metal with a universal value of the conductance [6–8].

Frustration in a quantum JJA can be introduced either by applying a magnetic field or by means of a gate voltage with respect to the ground plane. The effect of the *magnetic frustration* has been studied extensively in the classical limit [9]. The presence of the magnetic field induces vortices in the system and if the frustration is a rational number ($f \equiv \Phi/\Phi_0 = p/q$ where Φ is the magnetic flux piercing each plaquette and $\Phi_0 = h/2e$) then the ground state consists of a checkerboard configuration of vortices on a $q \times q$ cell. A particularly interesting case is the fully frustrated situation ($f = 1/2$) where the two degenerate ground states consist of vortex lattice with a 2×2 elementary supercell. The current corresponding to this vortex arrangement flows either clockwise or anticlockwise in each plaquette. We refer to this ϕ 's configuration as a *chiral* (ground) state. The effect of quantum fluctuations for JJA at $f = 1/2$ has been investigated in Ref. [10]: besides driving the SI transition at $T = 0$, quantum fluctuations affect also the superconducting regime. Indeed they reduce both the superconducting transition temperature and the magnitude of Josephson currents (though the modulus Δ of the order parameter is unchanged). However the configuration of the phases ϕ_i and the supercurrent flow patterns are unchanged so the ground state is still chiral.

Quantum effects may be modulated by means of a gate voltage to the ground V_x , which we denote as *charge frustration*. Indeed the energy difference for two charge states in each island with n and $n + 1$ extra electrons may be reduced by changing V_x . Consequently the effects of a finite charging energy are weakened and the superconducting region in the phase diagram turns out to be enlarged. In the presence of charge frustration and finite range Coulomb interaction, the phase diagram has a rather rich structure. For instance different Mott insulating phases are present. They are characterized by different crystal-like configuration of the extra charge on each island en_i which is arranged in superlattices whose lattice constant depends on V_x . In addition new *supersolid* phases may appear where off-diagonal (superfluid) and diagonal (charge-crystalline) long range order coexist. Since

the original prediction by Andreev and Lifshits [21] there were numerous works concerning the determination of the location and the size of these supersolid regions in the phase diagram [11–14]. Most of the theoretical investigations are restricted to the mean field approximation; a step beyond this, using Quantum Monte Carlo was done in Ref. [15] for the JJA Model and in Ref. [16] for the Bose-Hubbard model. The presence of the supersolid region is not an artifact of the mean field approximation though its size is substantially reduced due to the effect of fluctuations. Investigations in one dimensional systems [17] by means of Monte Carlo simulation do not show any trace of supersolid phase.

All these investigations concerning frustration in quantum arrays considered either charge *or* magnetic frustration. The combined effect of *both* frustration may lead to interesting effects. The most striking prediction is that for certain ratios of the magnetic to charge frustration the JJA will be in a Quantum Hall phase [18]. The proposal is rather suggesting although experiments are not yet available to support it and there is not a detailed study of the phase diagram which would allow to locate the region where the Quantum Hall phase should be observed.

Motivated by these facts we make a first step in this direction by studying the phase diagram and the low lying excitations of a JJA in the presence of both charge and phase frustration. In particular we will confine ourselves to the case of fully frustrated JJA for which the ground state is known in the classical limit. Although we cannot make still statements concerning the QHE already at this stage we find new interesting results. Two different supersolid phases are identified which we indicate as *chiral* (SS) and *Non-Chiral* (NCSS) supersolid. This NCSS is a new phase and has not a corresponding stable phase at $f = 0$.

The *whole* supersolid region is enlarged as compared to the case of zero magnetic field.

The paper is organized as follows. In the next section we introduce the Quantum Phase Model (QPM) commonly used to study JJA and reduce it in the standard way to the XXZ Heisenberg model. The phase diagram of the latter model is studied at mean field level in section III using the $1/S$ expansion. We would like to point out that the presence of both magnetic and charge frustrations makes the calculation non trivial already at this level and that it is impossible to use other standard tools as Monte Carlo simulations or the self-consistent harmonic approximation. In the case of Monte Carlo there are sign problems while in the harmonic approximation the discreteness of charges which is essential to describe supersolids is not accounted for. In section IV we study the spectrum of the low-lying excitations in all the regions of the phase diagram. Finally, section V is devoted to the conclusions.

II. THE MODEL

The physics of JJA made of submicron size junctions is usually described in terms of quantum dynamics of the phases ϕ_i (at low temperatures the fluctuations of the modulus Δ are unimportant). Since in nanofabricated samples there are no Ohmic currents between the islands and also quasiparticle tunneling is negligible all the relevant physics is captured by the QPM

$$H_{QP} = \sum_{i,j} (n_i - n_x) U_{ij} (n_j - n_x) - J \sum_{\langle i,j \rangle} \cos(\phi_i - \phi_j - A_{ij}) , \quad (1)$$

where n_i and ϕ_i are canonically conjugated with, $[\phi_i, n_j] = 2e i \delta_{ij}$. The Coulomb interaction is described by the matrix $U_{ij} = 4e^2 C_{ij}^{-1}$ where C_{ij} is the inverse of the capacitance matrix. The external voltage V_x enters via the induced charge en_x and fixes the average charge on each island. A perpendicular magnetic field with vector potential \mathbf{A} enters the QPM in the standard way through $A_{ij} = \frac{2e}{\hbar c} \int_i^j \mathbf{A} \cdot d\mathbf{l}$ and gives the magnetic frustration parameter $f = \frac{1}{2\pi} \sum A_{ij}$ where the summation runs on an elementary plaquette. In the classical limit, $J/U \rightarrow \infty$, JJA's are a physical realization of the two dimensional XY model.

We will consider very large *onsite* Coulomb interaction and very low temperatures where few charge states are important. In this limit the relevant physics is captured by considering only two charge states per island and the QPM is equivalent to a spin-1/2 Heisenberg model [11]

$$H_S = -h \sum_i S_i^z + \sum_{i,j} S_i^z U_{ij} S_j^z - J \sum_{\langle i,j \rangle} \left(e^{iA_{ij}} S_i^+ S_j^- + e^{-iA_{ij}} S_j^+ S_i^- \right), \quad (2)$$

where the operators S_i^z , S_i^+ , S_j^- are the usual $su(2)$ operators, S_i^z being related to the charge on each island ($n_i = S_i^z + \frac{1}{2}$), and the raising and lowering S_i^\pm operators corresponding to the "creation" and "annihilation" operators $e^{\pm i\phi_j}$ of the QPM. The "external" field h is defined as $h = (n_x - 1/2) \sum_{i,j} U_{i,j}$. A particularly interesting case is when n_x is close to a half integer and the two charge states are almost degenerate. The various magnetic orderings in the XXZ hamiltonian correspond to the different phases in the QPM: long range order in $\langle S^x \rangle$ and $\langle S^y \rangle$ ($\sqrt{\langle S_i^x \rangle^2 + \langle S^y \rangle^2} \neq 0$) indicates superfluidity in the QPM, while long range order in $\langle S^z \rangle$ ($|\langle S^z \rangle| \neq 0$) describes order in the charge configuration.

In order to treat the $f = 1/2$ case we consider a square lattice and use the gauge $\mathbf{A} = Hy\hat{x}$. This gives $A_{ij} = \pi \frac{y_i}{a} \text{sign}(x_j - x_i)$ where the coordinates of the neighbouring sites i and j appear and a is the lattice spacing. This is illustrated in Fig.(1) where the dashed lines indicate the antiferromagnetic bond ($A_{ij} = \pi$) and the continuous lines the ferromagnetic bonds ($A_{ij} = 0$).

In the classical limit there are two degenerate 2×2 periodic ground states: in the QPM language they correspond to two characteristic ϕ_i patterns (one of them is shown in Fig. 1) which determine a checkerboard arrangement of vortices and antivortices.

In the XXZ version this corresponds to $\langle S_i^x \rangle$ and $\langle S_i^y \rangle$ reproducing the above ϕ pattern, $\arctan(\langle S_i^y \rangle / \langle S_i^x \rangle) = \phi_i$ and $\sqrt{\langle S_i^x \rangle^2 + \langle S_i^y \rangle^2} = 1$. Charge are completely delocalized which corresponds to $\langle S_i^z \rangle = 0$.

In the rest of the paper we consider the Coulomb interaction only between nearest neighbour (U_1) and next nearest neighbour (U_2) sites.

III. PHASE DIAGRAM

In this section we obtain the phase diagram for $f = 1/2$ in the presence of arbitrary charge frustration. Previous work already established the phase diagram of the spin hamiltonian in zero magnetic field [11–13,16]. The chiral configuration of the classical ground states suggests the introduction of four sublattices indicated by the index $l = \alpha, \beta, \gamma, \delta$ (Fig. 1). Each site is parametrized by l and an additional index p which runs within each sublattice.

We now focus on the XXZ model which we study using the $1/S$ -expansion (S is the modulus of the spin vector). First the quantization axis in each sublattice is rotated to align the spins along the direction of the relative magnetization. We obtain the rotated hamiltonian $\mathbf{R}H_S\mathbf{R}^{-1}$, where

$$\mathbf{R} \doteq \prod_p \prod_{l=\alpha, \beta, \gamma, \delta} R^z_{pl} R^x_{pl}, \quad (3)$$

with $R^z_{pl} \doteq e^{i\phi_l S^z_{pl}}$, $R^x_{pl} \doteq e^{i\theta_l S^x_{pl}}$. Then we perform the $1/S$ expansion and determine the actual values of the eight angles ϕ_l and θ_l by minimizing the $S \rightarrow \infty$ limit H_∞ of the rotated hamiltonian. The above procedure allows to characterize ground states whose properties are uniform within each sublattice. The order parameters will be $\sin\theta_l$ for global phase coherence and $\cos\theta_l$ for charge ordering. The ϕ_l configuration will determine the supercurrent configuration in the flux phases.

The $1/S$ expansion of the rotated hamiltonian can be carried on sistematically by using the Holstein-Primakoff transformation $S^+_{pl} = \sqrt{2S} a_{pl}^\dagger \sqrt{1 - n_{pl}/S}$, $S^-_{pl} = (S^+_{pl})^\dagger$, $S^z_{pl} = n_{pl} - S$, where a_{pl} , a_{pl}^\dagger are bosons, and $n_{pl} = a_{pl}^\dagger a_{pl}$. These operators describe excitations around the $S \rightarrow \infty$ ground state (and *not* particles in the QPM). We obtain

$$\mathbf{R}H_S\mathbf{R}^{-1} = H_\infty + H_{SW} + \mathcal{O}(\sqrt{S}). \quad (4)$$

where H_∞ is of order S^2 , H_{SW} describes low energy fluctuations around the $S \rightarrow \infty$ ground state and turns out to be of order S . The $S \rightarrow \infty$ ground state properties are obtained by minimizing H_∞ which is a sum over p of identical terms of the form

$$H_\infty = \frac{N}{4} \sum_l \left[-\frac{h}{2} \cos \theta_l + \frac{U_1}{8} \cos \theta_l \sum_{m=nn(l)} \cos \theta_m + \frac{U_2}{4} \cos \theta_l \sum_{m=nnn(l)} \cos \theta_m - \frac{J}{4} \sin \theta_l \sum_{m=nn(l)} e^{A_{lm}} \sin \theta_m \cos(\phi_l - \phi_m) \right] \quad (5)$$

The minimization of the H_∞ leads to eight equations in the variables ϕ_l and θ_l defined on the plaquette of Fig.(1.b). Four of these equations can be solved analitically with the result

$$\begin{aligned} \tan(\phi_\gamma - \phi_\beta) &= \frac{\sqrt{16a^2b^2 - (b^2 - 1)(a^2 - 1)}}{(b^2 - 1)(a^2 + 1)}, \\ \tan(\phi_\delta - \phi_\alpha) &= -\frac{\sqrt{16a^2b^2 - (b^2 - 1)(a^2 - 1)}}{(a^2 - 1)(b^2 + 1)}, \\ \tan(\phi_\beta - \phi_\alpha) &= -\frac{\sqrt{16a^2b^2 - (b^2 - 1)(a^2 - 1)}}{(a^2 - 1)(b^2 + 1) - 2b^2(a^2 + 1)}. \end{aligned} \quad (6)$$

where

$$a = \frac{\sin \theta_\alpha}{\sin \theta_\delta}, \quad b = \frac{\sin \theta_\beta}{\sin \theta_\gamma}$$

We now look for solutions with $a = b = 1$ which correspond to phases with checkerboard simmetry. The resulting configuration of the ϕ_l is the same as in the classical limit, so

the supercurrent has the same chiral pattern. the ground state is chiral as in the classical situation. This has been noticed in the case of zero external charge in Ref [10]. We show that for non zero charge frustration the above conclusion holds true for the superfluid phase and for the chiral SS supersolid.

The remaining equations for θ_l reduce to the ones of the $f = 0$ case with the substitution $J \rightarrow \frac{\sqrt{2}}{2}J$; the solutions then read

$$\cos \theta = \frac{h}{2(U_1 + U_2 + \sqrt{2}J)}. \quad (7)$$

for the superfluid (SF) and

$$\begin{cases} \cos \theta_\alpha \\ \cos \theta_\beta \end{cases} = \begin{cases} \frac{1}{2} \left(v + \sqrt{v^2 - 4w} \right) \\ \frac{1}{2} \left(v - \sqrt{v^2 - 4w} \right) \end{cases}, \quad (8)$$

the chiral SS supersolid. We defined $w \doteq (h - h_s)/(2U_2\kappa)$, $h_s \doteq 2\sqrt{(U_1 - U_2)^2 - 2J^2}$, $\kappa \doteq \sqrt{1 - \left[\sqrt{2}J/(U_1 - U_2) \right]^2} (1 + w)$.

By comparing the energies relative to the above solutions we obtain the boundaries between the phases with checkerboard symmetry

Paramagnetic - canted state

$$h = \pm 2(U_1 + U_2 + \sqrt{2}J), \quad (9)$$

Canted state - $\frac{1}{4}$ or $\frac{3}{4}$ lobe

$$h = \pm \left[U_1 + U_2 + \sqrt{2}J + \sqrt{(U_1 + U_2 + \sqrt{2}J)(U_1 + U_2 - 3\sqrt{2}J)} \right], \quad (10)$$

Canted - chiral supersolid state

$$h = 2(U_1 + U_2 + \sqrt{2}J) \sqrt{\frac{(U_1 - U_2 - \sqrt{2}J)}{(U_1 - U_2 + \sqrt{2}J)}}, \quad (11)$$

Chiral supersolid state - Nèel state

$$h = 2\sqrt{(U_1 - U_2)^2 - 2J^2}, \quad (12)$$

Chiral supersolid - $\frac{1}{4}$ or $\frac{3}{4}$ lobes

$$h = \pm \left[2U_2 + h_s - \sqrt{(2U_2 + h_s)^2 - h_s^2 - 8U_2(U_1 - U_2)} \right]. \quad (13)$$

The spin configurations corresponding to the insulating, superfluid and supersolid regions are shown in Figs.(2). In the Mott lobes there is no projection of the spin on the xy plane and the three spin configurations in Fig.(2.a) correspond to filling 1, 1/2 and 3/4. In Fig.(2.b)

and Fig.(2.c) the superfluid and supersolid regions are represented. The fact that the ϕ configuration is not affected by quantum fluctuations has already been noticed in Ref. [10] for zero external charge. We extend this result to the SF and SS phases resulting at non zero charge frustration. However we discuss below the NCSS solution which does not show the above supercurrent pattern.

The NCSS ground state is found if we look for solutions with no checkerboard symmetry. A non-checkerboard phase was also found at $f = 0$ by Bruder *et al* [] and was named SS2 supersolid. We find two degenerate NCSS configurations namely $\phi_\alpha = \phi_\beta = \phi_\gamma = 0$ (ϕ_δ is meaningless since $\sin\theta_\delta$ turns out to vanish) and $\phi_\alpha = 0, \phi_\beta = \phi_\delta = \pi, (\sin\theta_\gamma = 0)$. We obtained the regions of the phase diagram where the NCSS solution is stable by minimizing numerically the energy (5). The resulting pattern of the supercurrent is different from the classical chiral one. We point out that in this case the equations for the angles θ_l cannot be obtained from the $f = 0$ equations by simply rescaling $J \rightarrow J/\sqrt{2}$.

The solutions are characterized by the $\sin\theta$ order parameter vanishing on one of the four sublattices. On this particular sublattice $\cos\theta = 1$ so the charge is well defined. Thus the NCSS ground state describes a supersolid, since charge-crystalline and superfluid order coexist, but the chiral supercurrent pattern is lost. The phase boundaries obtained numerically and the configurations of the angles ϕ_l and θ_l of the NCSS ground state are shown in Fig.(2.d).

All the phase boundaries obtained in this section are summarized in the phase diagram shown in Fig.(3). The *whole* supersolid region (SS and NCSS phases) is enlarged compared to the $f = 0$ case (SS1 and SS2 phases). At $f = 0$ the tip of the lobe (which coincides with the extension of the supersolid phase in the hard core limit) will correspond to $J/U_1 = 0.45$. A blow-up of the NCSS region is shown in Fig.(4) and compared with the rescaled $f = 0$ phase diagram. This figure emphasizes that although the *whole* supersolid region is obtained by rescaling the $f = 0$ phase diagram, the individual phases are not (the rescaled SS2-SS1 phase boundary is shown by crosses).

IV. EXCITATION SPECTRA

The excitation spectra can be obtained calculating the eigenmodes of H_{SW} . As pointed out in the previous section all the terms up to $\mathcal{O}(S)$ are retained in the $1/S$ -expansion; this, in turns, corresponds to retain products at most bilinear of the creation and annihilation operators. If we regarded l as a colour index, H_{SW} describes a system of four kinds of interacting l -bosons defined on a lattice whose sites are labeled by the index p . Then we Fourier transform with respect to p and H_{SW} reduces to a sum of single mode hamiltonians

$$\begin{aligned}
H_{SW} &= \sum_k H_k, \\
H_k &= \left(\varepsilon_k^{(\alpha,\beta)} + \varepsilon_k^{(\alpha,\gamma)} + \varepsilon_k^{(\alpha,\delta)} \right) n_{k,\alpha} + \left(\varepsilon_k^{(\alpha,\beta)} + \varepsilon_k^{(\beta,\delta)} + \varepsilon_k^{(\beta,\gamma)} \right) n_{k,\beta} + \\
&\quad \left(\varepsilon_k^{(\alpha,\gamma)} + \varepsilon_k^{(\gamma,\delta)} + \varepsilon_k^{(\beta,\gamma)} \right) n_{k,\gamma} + \left(\varepsilon_k^{(\alpha,\delta)} + \varepsilon_k^{(\beta,\delta)} + \varepsilon_k^{(\gamma,\delta)} \right) n_{k,\delta} + \\
&\quad \left(v_k^{(\alpha,\gamma)} a_{k,\alpha}^\dagger a_{k,\gamma} + v_k^{(\alpha,\gamma)*} a_{k,\gamma}^\dagger a_{k,\alpha} \right) + \left(v_k^{(\alpha,\beta)} a_{k,\alpha}^\dagger a_{k,\beta} + v_k^{(\alpha,\beta)*} a_{k,\beta}^\dagger a_{k,\alpha} \right) + \\
&\quad \left(v_k^{(\beta,\delta)} a_{k,\beta}^\dagger a_{k,\delta} + v_k^{(\beta,\delta)*} a_{k,\delta}^\dagger a_{k,\beta} \right) + \left(v_k^{(\gamma,\delta)} a_{k,\gamma}^\dagger a_{k,\delta} + v_k^{(\gamma,\delta)*} a_{k,\delta}^\dagger a_{k,\gamma} \right) +
\end{aligned}$$

$$\begin{aligned}
& \left(v_k^{(\alpha,\delta)} a_{k,\alpha}^\dagger a_{k,\delta} + v_k^{(\alpha,\delta)*} a_{k,\alpha}^\dagger a_{k,\delta} \right) + \left(v_k^{(\beta,\gamma)} a_{k,\beta}^\dagger a_{k,\gamma} + v_k^{(\beta,\gamma)*} a_{k,\gamma}^\dagger a_{k,\beta} \right) + \\
& \left(q_k^{(\alpha,\gamma)} a_{k,\alpha}^\dagger a_{k,\gamma}^\dagger + q_k^{(\alpha,\gamma)*} a_{k,\gamma} a_{k,\alpha} \right) + \left(q_k^{(\alpha,\beta)} a_{k,\alpha}^\dagger a_{k,\beta}^\dagger + q_k^{(\alpha,\beta)*} a_{k,\beta} a_{k,\alpha} \right) + \\
& \left(q_k^{(\beta,\delta)} a_{k,\beta}^\dagger a_{k,\delta}^\dagger + q_k^{(\beta,\delta)*} a_{k,\beta} a_{k,\delta} \right) + \left(q_k^{(\gamma,\delta)} a_{k,\gamma}^\dagger a_{k,\delta}^\dagger + q_k^{(\gamma,\delta)*} a_{k,\gamma} a_{k,\delta} \right) + \\
& \left(q_k^{(\alpha,\delta)} a_{k,\alpha}^\dagger a_{k,\delta}^\dagger + q_k^{(\alpha,\delta)*} a_{k,\alpha} a_{k,\delta} \right) + \left(q_k^{(\beta,\gamma)} a_{k,\beta}^\dagger a_{k,\gamma}^\dagger + q_k^{(\beta,\gamma)*} a_{k,\gamma} a_{k,\beta} \right) , \tag{14}
\end{aligned}$$

The coefficients in the hamiltonian (14) (reported in the Appendix A) depend on the angles θ_l and ϕ_l introduced in the section III. The k -sum is restricted to half of the Brillouin zone because of the doubling of the lattice constant due to the magnetic frustration. Linear contributions in the operators $a_{k,i}^\dagger, a_{k,i}$ vanish for the $\{\theta_l, \phi_l\}$ ground state configuration.

The hamiltonian H_{SW} is diagonalized using an algebraic technique [23,25] briefly described below: we introduce the following operators

$$\begin{aligned}
X_{ll'} & \doteq a_{k,l} a_{-k,l'} + a_{k,l'} a_{-k,l} , \\
X^{ll'} & \doteq a_{k,l'}^\dagger a_{-k,l}^\dagger + a_{k,l}^\dagger a_{-k,l'}^\dagger = (X_{ll'})^\dagger , \\
X_l^{l'} & \doteq a_{k,l'}^\dagger a_{k,l} + a_{-k,l'}^\dagger a_{-k,l} , \\
X_{l'}^l & \doteq a_{k,l}^\dagger a_{k,l'} + a_{-k,l}^\dagger a_{-k,l'} = (X_l^{l'})^\dagger , \\
X_l^l & \doteq n_{k,l} + n_{-k,l} + 1 , \tag{15}
\end{aligned}$$

which obey the following commutation rules

$$\begin{aligned}
[X_{ll'}, X_{mm'}] & = [X^{ll'}, X^{mm'}] = 0 \\
[X_{ll'}, X^{mm'}] & = X_l^m \delta_{l'}^{m'} + X_l^{m'} \delta_{l'}^m + X_{l'}^m \delta_l^{m'} + X_{l'}^{m'} \delta_l^m , \\
[X_{ll'}, X_m^{m'}] & = X_{lm} \delta_{l'}^{m'} + X_{l'm} \delta_l^{m'} , \\
[X^{ll'}, X_m^{m'}] & = -X^{lm'} \delta_m^{l'} - X^{l'm'} \delta_m^l , \\
[X_l^{l'}, X_m^{m'}] & = X_m^{l'} \delta_l^{m'} - X^{lm'} \delta_m^{l'} , \tag{16}
\end{aligned}$$

where we have omitted the k -index in the X 's and $\{l, l', m, m'\}$ are colour indices. The 36 operators $\{X_{ll'}, X^{ll'}, X_l^{l'}, X_{l'}^l, X_l^l\}$ form a base for the non-compact symplectic Lie algebra $sp(8)_k$ [22]. The diagonal operators X_l^l generate the Cartan subalgebra of $sp(8)_k$ whose dimension is 4 (equal to the rank of the algebra). The other off-diagonal operators, in number of 32, are the non-Cartan generators of the algebra. By using the definitions of Eq.(15), one can see that H_k belongs to $sp(8)_k$ since it can be written as linear combination of a subset of its generators

$$H_k = \sum_l D_{ll}^{(k)} X_l^l + \sum_{l \neq l'} D_{ll'}^{(k)} X_l^{l'} + \sum_{l \neq l'} R_{ll'}^{(k)} X_{ll'} , \tag{17}$$

where $R_{ll'}^{(k)} = R_{l'l}^{(k)*}$ and $D_{ll'}^{(k)} = D_{l'l}^{(k)*}$. (The coefficients in the expression (17) are listed in the Appendix B). Eq.(17) suggests that H_{SW} possesses $\mathcal{A} = \bigoplus_k sp(8)_k$ as dynamical algebra, therefore we can diagonalize the Hamiltonian using the fundamental faithful (*i.e.* preserving the commutation rules) Irreducible Representation (IRR) of \mathcal{A} . It is worthwhile to notice that because of the non compactness of $sp(8)$, every finite dimensional IRR of such

algebra is not hermitian [27]. Despite of this fact we can use IRR of \mathcal{A} in order to obtain the correct eigenvalues of H_{SW} (see Appendix A). Such eigenvalues still depend on θ_l and ϕ_l : the actual spectra in the various phases are worked out by specifying the correspondent $S \rightarrow \infty$ ground state $\{\theta_l, \phi_l\}$ configuration for each phase. The main results of this procedure are described below for the various regions of the phase diagram.

Insulating phases: Since the superfluid order parameter is zero there is no effect due to magnetic frustration. The Neél and insulating $\frac{1}{4}$ (and $\frac{3}{4}$) phases are charge-modulated solids. The lowest lying excitations are gapped and particle like. They correspond to particle - hole excitations. In Fig. (5.a) and Fig. (5.b) we show the spectrum for the 1/2 and 3/4 lobes. The Neél solid is charge-modulated along both x and y directions and the gapped branches are shown in Fig. (5.a). The four branches in the 3/4 lobe come from the more complicated structure of the elementary cell. In this state the transverse phonon like excitation, characteristic of the diagonal long range order along rows and/or columns (where the charge is uniform) In addition we find the particle like spectrum (with positive curvature at small k) which reflects charge modulation. This is shown in Fig. (5.b) where the the dashed branch represents the phonon like excitation.

The Mott phases are not modulated in any direction, then the low lying excitations are phonon like .

SF phase: Because of the doubling of the elementary cell of the lattice due to the magnetic field, a gapped branch is present in addition to a gapless mode which linearly depend on k at small k , see Fig. (6). This was already discussed in the classical case by Ariosa *et al.* [9]). Long range diagonal order existing along any lattice direction induces transverse phonon like excitations.

Supersolid SS phase: In the SS phase both diagonal and off-diagonal order modulation are present. In this state the in-phase density fluctuations are coupled to the off-diagonal fluctuations and decreases the sound velocity because it reduces the superfluid density. The supersolid is characterized also by a modulation of the charge. Such modulation of the number of particles can be considered as defects of the lattice and their oscillations can be regarded as a fluctuation of the diagonal order on each site [19]. The localized quasi-particle associated to the collective oscillations of the defects were termed as *defectons* [21]. The gapped branch reveals the particle like excitations consistently with this physical picture. In Fig.(7) the acoustic branch is reminiscent of the superfluid order while the gapped branch with positive curvature is the excitation spectrum for the defectons.

NCSS phase: As in the previous case, the off-diagonal order is coupled with the density waves, but in this state there are four branches. The gapless one, reflects the superfluid nature of this state. Since the mean field superfluid order parameter vanishes in a lattice site of the 2×2 plaquette the sound velocity is strongly decreased. Two of the three gapped curves take into account the defects of the lattice, the other one means that in the system there are transverse phase-phonon excitations too. This is summarized in in Fig.(8).

An important issue which can be addressed by studying the excitation spectrum is the determination of the dynamical critical exponent at the various phase boundaries. It turns out that the fully frustration does not change the critical exponents at the phase boundaries. At the SS -Neél solid transition the gap of the lower branch of the solid vanishes as k^2 giving a critical exponent $z = 2$ [16]. At the SF- SS supersolid transition the critical mode is $k = (\pi, \pi)$ and the roton minimum is at this wave vector. At the phase boundary the roton

gap disappears linearly in k giving $z = 1$.

V. CONCLUSIONS

In this paper we considered the properties of a fully frustrated quantum Josephson Junction array in the presence of arbitrary charge frustration. We determined the mean field phase diagram at $T = 0$ as well as the low lying excitation spectrum using a $1/S$ expansion for the equivalent XXZ model.

At $f = 1/2$ two kinds of supersolid phases, in addition to the ordinary superfluid and insulating phases, are present. Besides the chiral supersolid SS which has an analog in the absence of magnetic frustration we find the new NCSS supersolid phase which is non chiral. In the case of the superfluid and the SS supersolid the main effect of quantum fluctuation and charge frustration is to lower in magnitude the superfluid order parameter. The supercurrent pattern induced by the external magnetic field is however unaffected. In our mean field analysis this is reflected in a rescaling of J . In other words the magnetic frustration fixes the current distribution while the charge frustration is responsible for the reduction of the magnitude of the superfluid order parameter. In the non chiral supersolid NCSS diagonal and off-diagonal long range order coexist in a non trivial way and the combined effect of charge and magnetic frustration cannot be separated as in the other phases. The NCSS ground state has no checkerboard symmetry since the superfluid order parameter vanishes in one of the four sites of each plaquette and two flux quanta may be accommodated in four neighboring plaquettes. There is non chiral symmetry in this phase. The NCSS phase exists only in the fully frustrated case and has no analog at $f = 0$. The *whole* (SS plus NCSS) supersolid region in the phase diagram is enlarged compared to the unfrustrated case: the supersolid state better adjust to the periodicity (on a 2×2 plaquettes elementary cell) induced by magnetic frustration than the SF phase and it is more favoured than in the $f = 0$ case. This may be important for the experiments because the combination of charge and magnetic frustration may help in detecting the supersolid phase.

We also determined the low lying excitation spectrum of the system. Due to the combined presence of magnetic and charge frustration the excitation spectra become more structured. They can be revealed, for instance, by studying the anomalies in the $I - V$ characteristics when Andreev current is injected into the array is coupled from a normal metal electrode [29].

We are currently investigating different rational values of the magnetic frustration in order to study the possibility of a Quantum Hall phase as predicted in Ref. ([18]).

ACKNOWLEDGMENTS

We would like to thank C. Bruder, A. van Otterlo, K.H. Wagenblast, M. Rasetti, G. Schön, G.T. Zimanyi for useful discussions. The financial support of the European Community (HCM-network CHRX-CT93-0136) and of INFN (Italy) is gratefully acknowledged. Two of us (R.F and G.F.) acknowledge the warm hospitality of the Institut für Theoretische Festkörperphysik (Karlsruhe) where part of the work was performed.

APPENDIX A:

In this Appendix we list the coefficients of the hamiltonian (14)

$$\begin{aligned}\varepsilon_k^{(l,m)} &\doteq 2te^{iA_{lm}} \sin \theta_l \sin \theta_m \cos z_{l,m} - \cos \theta_l \cos \theta_m , \\ \varepsilon_k^{(l,n)} &\doteq -2U_2 \cos \theta_l \cos \theta_m .\end{aligned}\tag{A1}$$

The coefficients of the off diagonal operators are

$$\begin{aligned}v_k^{(l,m)} &\doteq \cos(\mathbf{k} \cdot \mathbf{a}_{l,m}) \left\{ te^{iA_{lm}} [(\cos \theta_l \cos \theta_m + 1) \cos z_{l,m} - i(\cos \theta_l + \cos \theta_m) \sin z_{l,m}] + \right. \\ &\quad \left. \frac{1}{2} \sin \theta_l \sin \theta_m \right\} , \\ v_k^{(l,n)} &\doteq U_2 \cos k_y \cos k_x \sin \theta_l \sin \theta_m \\ q_k^{(l,m)} &\doteq \cos(\mathbf{k} \cdot \mathbf{a}_{l,m}) \left\{ te^{iA_{lm}} [(\cos \theta_l \cos \theta_m - 1) \cos z_{l,m} + i(\cos \theta_l + \cos \theta_m) \sin z_{l,m}] + \right. \\ &\quad \left. \frac{1}{2} \sin \theta_l \sin \theta_m \right\} , \\ q_k^{(l,m)} &\doteq -U_2 \cos k_y \cos k_x \sin \theta_l \sin \theta_m\end{aligned}\tag{A2}$$

where l and n indicate $n.n.$ and $n.n.n.$ sites respectively. In the preceding expressions the lattice spacing vector $\mathbf{a}_{l,m}$ has both normalized components and $z_{l,m}$ are the superfluid order parameter's out of phase ($\phi_l - \phi_m$) on nearest neighbour sites. In the present case the coefficients (A2) are \mathbf{C} -numbers and they reduce to real ones in the zero magnetic field case only.

APPENDIX B:

The IRR faithful representation of $sp(8)$ we used consists in mapping the hamiltonian H_{SW} in the matrix $\mathcal{M}(H_{SW})$. Since that $sp(8)$ is a non compact algebra \mathcal{M} turns to be not hermitian and it has the following structure (we use the same notation as in Ref. [28])

$$\begin{pmatrix} \mathcal{D} & \mathcal{R} \\ -\mathcal{R} & -\tilde{\mathcal{D}} \end{pmatrix}\tag{B1}$$

where the tilde indicates the reflection in the minor diagonal ($\tilde{\mathcal{R}} = \mathcal{R}$) and \mathcal{D} is hermitian. The matrix elements of \mathcal{D} are

$$\begin{aligned}D_{11}^{(k)} &\doteq \frac{1}{2} \left(\varepsilon_k^{(\alpha,\gamma)} + \varepsilon_k^{(\alpha,\beta)} + \varepsilon_k^{(\alpha,\delta)} + h \cos \theta_\alpha \right) , \\ D_{22}^{(k)} &\doteq \frac{1}{2} \left(\varepsilon_k^{(\alpha,\beta)} + \varepsilon_k^{(\beta,\delta)} + \varepsilon_k^{(\beta,\gamma)} + h \cos \theta_\beta \right) , \\ D_{33}^{(k)} &\doteq \frac{1}{2} \left(\varepsilon_k^{(\alpha,\beta)} + \varepsilon_k^{(\beta,\delta)} + \varepsilon_k^{(\beta,\gamma)} + h \cos \theta_\beta \right) , \\ D_{44}^{(k)} &\doteq \frac{1}{2} \left(\varepsilon_k^{(\gamma,\delta)} + \varepsilon_k^{(\beta,\delta)} + \varepsilon_k^{(\alpha,\delta)} + h \cos \theta_\delta \right) .\end{aligned}\tag{B2}$$

$$\begin{aligned}
D_{12}^{(k)} &\doteq \frac{1}{2}v_k^{(\alpha,\beta)} , & D_{13}^{(k)} &\doteq \frac{1}{2}v_k^{(\alpha,\gamma)} , & D_{14}^{(k)} &\doteq \frac{1}{2}v_k^{(\alpha,\delta)} , \\
D_{23}^{(k)} &\doteq \frac{1}{2}v_k^{(\beta,\gamma)} , & D_{24}^{(k)} &\doteq \frac{1}{2}v_k^{(\beta,\delta)} , & D_{34}^{(k)} &\doteq \frac{1}{2}v_k^{(\gamma,\delta)} .
\end{aligned} \tag{B3}$$

The matrix \mathcal{R} has the following structure

$$\begin{pmatrix} R_{14} & R_{13} & R_{12} & 0 \\ R_{24} & R_{23} & 0 & R_{21} \\ R_{34} & 0 & R_{32} & R_{31} \\ 0 & R_{43} & R_{42} & R_{41} \end{pmatrix} \tag{B4}$$

and its elements are given below

$$\begin{aligned}
R_{12}^{(k)} &\doteq \frac{1}{2}q_k^{(\alpha,\beta)} , & R_{13}^{(k)} &\doteq \frac{1}{2}q_k^{(\alpha,\gamma)} , & R_{14}^{(k)} &\doteq \frac{1}{2}q_k^{(\alpha,\delta)} , \\
R_{23}^{(k)} &\doteq \frac{1}{2}q_k^{(\beta,\gamma)} , & R_{24}^{(k)} &\doteq \frac{1}{2}q_k^{(\beta,\delta)} , & R_{34}^{(k)} &\doteq \frac{1}{2}q_k^{(\gamma,\delta)} .
\end{aligned} \tag{B5}$$

The diagonalization of H_{SW} is equivalent to an inner automorphism of the algebra on itself. In other words, we can define the unitary operator $\mathbf{U} \doteq \prod_k U_k$, with

$$U_k \doteq e^{G_k} , \tag{B6}$$

where the antihermitian operator G_k is a linear combination of the non-Cartan generators of the algebra

$$G_k \doteq \sum_{r,s} [\psi_{r,s} (X_{rs} - X^{rs}) + \psi_r^s (X_r^s - X_s^r)] . \tag{B7}$$

The rotation of the hamiltonian trough \mathbf{U} defines an inner automorphism of the algebra generalizing the Bogoliubov transformation

$$\begin{aligned}
\mathbf{U}H_{SW}\mathbf{U}^{-1} &= \sum_k \exp(ad G_k) H_k , \\
\exp(ad G_k) H_k &\doteq U_k H_k U_k^{-1} \\
&= H_k + \sum_n \frac{1}{n!} [\dots[G_k, [G_k, H_k]]\dots] ,
\end{aligned} \tag{B8}$$

For the closure property of the Lie algebras the equation (B8) still produce an element of \mathcal{A} , however we can fix the ψ_{rs} 's and the ψ_r^s 's in such a way to put to zero the coefficients of the off-diagonal part of the hamiltonian. As a final result H_{SW} becomes proportional to the generators of the Cartan subalgebra of \mathcal{A}

$$\mathbf{U}H_{SW}\mathbf{U}^{-1} = H_{DIAG.} = \sum_{r=1}^4 \omega_k^{(r)} X_r^r \tag{B9}$$

In the present case H_{SW} should be diagonal after having solved 16 coupled non linear equations. Being interested in the eigenvalues only, we are allowed to use the faithful representation of \mathcal{A} to find the spectrum of the hamiltonian diagonalizing the matrix $\mathcal{M}(H_{SW})$ instead of H_{SW} as operator using the equation (B8). These operations are equivalent because the diagonalization procedure involves commutators between the elements of the algebra only.

REFERENCES

- [1] Proceedings of the NATO Advanced Research Workshop on *Coherence in superconducting networks*, J.E. Mooji and G.Shön Eds., Physica **B152** (1988)
- [2] Proc. of the Conference on *Macroscopic quantum phenomena and coherence in superconducting networks* C. Giovannella and M. Tinkham Eds. , World Scientific (Singapore, 1995)
- [3] L.J. Geerligs, M. Peters, L.E.M. de Groot, A. Verbruggen, and J.E. Mooij, Phys. Rev. Lett. **63**, 326 (1989); H.S.J van der Zant, L.J. Geerligs, and J.E. Mooij, Europhys. Lett. **19**, 541 (1992); C.D. Chen, P. Delsing, D.B. Haviland, Y.Harada, and T. Claeson, Phys. Rev. **B50**, 3959 (1995).
- [4] K.B. Efetov Sov. Phys. JETP **51**, 1015 (1980); S. Doniach, Phys. Rev. B **24**, 5063 (1981); R.Fazio and G. Schön, Phys. Rev. B **43**, 5307 (1991).
- [5] M.P.A. Fisher, B. P. Weichman, G. Grinstein, and D. S. Fisher, Phys. Rev. B **40**, 546 (1989). G. G. Batrouni, R. T. Scalettar, and G. T. Zimanyi, Phys. Rev. Lett. **65**, 1765 (1990); W. Krauth and N. Trivedi, Europhys. Lett. **14**, 627 (1991).
- [6] M.P.A. Fisher, G. Grinstein and S.M. Girvin, Phys. Rev. Lett. **64**, (1990) 587.
- [7] X.G. Wen and A. Zee, Int.J.Mod.Phys. **B4**, 437 (1990).
- [8] M.-C. Cha, M.P.A. Fisher, S.M. Girvin, M. Wallin, A.P. Young, Phys. Rev. B **44**, (1991) 6883; M. Wallin, E.S. Sørensen, S.M. Girvin, and A.P. Young, Phys. Rev. **B45**, 13136 (1992); G.G. Batrouni, B. Larson, R.T. Scalettar, J. Tobochnik, and J. Wang, Phys. Rev. **B48**, 9628 (1993); A. van Otterlo, K.-H. Wagenblast, R. Fazio, and G. Schön, Phys. Rev. **48** (1993) 3316; R. Fazio and D. Zappalà, Phys. Rev. **B53**, R8883 (1996).
- [9] S. Teitel and C. Jayaprakash, Phys. Rev. **27** (1983) 598; S. Teitel and C. Jayaprakash, Phys. Rev. Lett. **51** (1983) 1999; T.C. Halsey, Phys. Rev. **B 31** (1985) 5728; W. Y. Shih and D. Stroud, Phys. Rev. B **30** 6774, (1984); W. Y. Shih and D. Stroud, Phys. Rev. B **28** 6575, (1983); D. Ariosa, A. Vallat and H. Beck., J. Phys. France **51**, (1990)
- [10] Fishman, R. S. and Stroud, D., Phys. Rev. B **37** 1499, (1987)
- [11] K.S. Liu and M.E. Fisher, J. Low Temp. Phys. **10**, 655 (1973).
- [12] H. Matsuda and T. Tsuneto, Suppl. Prog. Theor. Phys. **46**, 411 (1970).
- [13] C. Bruder, R. Fazio, and G. Shön, Phys. Rev. B **47**, 342 (1993).
- [14] E. Roddick and D.H. Stroud, Phys. Rev. B **48** 16600 (1993).
- [15] A. van Otterlo, K-H. Wagenblast, Phys. Rev. Lett. **48**, 16600 (1994).
- [16] R.T. Scalettar, G.G. Batrouni, A.P. Kampf, G.T. Zimanyi Phys. Rev. B **51** 8467 (1995).
- [17] P. Niyaz, R.T. Scalettar, C.Y. Fong and G.G. Batrouni, Phys. Rev. B **44** 7143 (1991)
- [18] A. Stern Phys. Rev. B **50** 10092 (1994); A.A. Odintsov and Yu. N. Nazarov Physica **B203**, 513 (1994) and Phys. Rev. B **51** 1133 (1995); M.Y. Choi Phys. Rev. B **50** 10088 (1994).
- [19] Y.C. Cheng, Phys. Rev. B **23**, 157 (1981).
- [20] G.Chester, Phys. Rev. A **2** 256, (1970).
- [21] A.F. Andreev, I.M. Lifshitz, Sov.Phys. *JETP* **29**, 1107 (1969)
- [22] Perelomov, A. M., 1986 *Generalized Coherent States and their Applications*, (Springer, Berlin).
- [23] Wybourne B.G. 1974 *Classical Groups for Physicist*, J.Wiley & Sons.
- [24] A.I. Solomon, J. Phys. A **14** (1981).
- [25] A. Montorsi, M. Rasetti, A.I. Solomon, Phys. Rev. Lett. **59** 2243 (1987).

- [26] L. Amico, M. Rasetti, R. Zecchina, to appear in *Physica* **A**.
- [27] Gilmore R.,1974 *Lie Groups, Lie Algebra, and some of Their Applications* J.Wiley & Sons.
- [28] W.-M. Zhang, D.H. Feng and R. Gilmore, *Rev. Mod. Phys.* **62**, 867 (1990).
- [29] G. Falci, R. Fazio, A. Tagliacozzo, and G. Giaquinta, *Europhys. Lett* **30**, 169 (1995)

FIGURES

FIG. 1. Due to the non trivial periodicity due to the magnetic frustration a 2×2 cell should be considered. The labels for the sites as used in the paper are here reported a). Using periodicity boundary conditions, as shown in a), one can reduce the problem defined on the plaquette drawn in b).

FIG. 2. The 3-components spin vectors we used are characterized by the usual Euler angles θ and ϕ . a) In the insulating phases the order parameter vanishes and only the θ configuration is important. b) The mean field order parameter's phase configuration is unaffected by magnetic frustration. c) The θ and ϕ configurations in the supersolid SS . As in the superfluid state, the magnetic frustration preserves the chiral order of the ground state. d) The two degenerate ground states of the NCSS. The circle indicates the lattice site where the phase of the superfluid order parameter is not defined.

FIG. 3. The phase diagram for the fully frustrated JJA. The *n.n.n.* Coulomb interaction is $U_2 = 0.1 U_1$.

FIG. 4. The region of the phase diagram containing the NCSS is shown in detail. In addition we report (with crosses) the phase boundary that should have the chiral supersolid $SS2$ by rescaling J as discussed in the text.

FIG. 5. a) The excitation spectrum of the Neèl insulator. at $J = U_1/4$, $U_2 = 3U_1/8$ and $h = 2U_1/3$. The behaviour at small k reveals the particle like nature of the excitations. In b) we show the four branches of the "3/4" insulating phase ($U_2 = 0.1U_1$, $h = 2U_1$ and $J = 0.1U_1$). The two lower curves have been rescaled by a factor 10.

FIG. 6. The acoustic and transverse phonon like branches in the superfluid are shown for $J = 1U_1$, $U_2 = 0.1 U_1$, $h = 2.2 U_1$, $k_y = 0$.

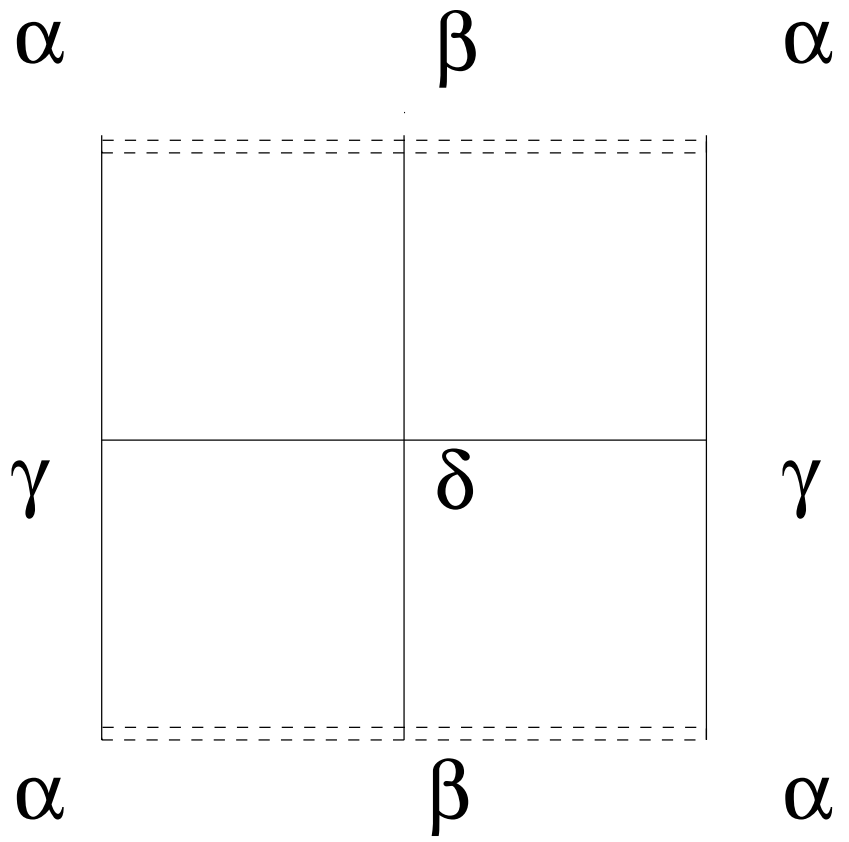
FIG. 7. In this figure we show the dispersion relations in supersolid SS ($J = 0.35U_1$, $U_2 = 0.1U_1$, $h = 1.7U_1$, $k_y = 0$). The sound velocity of the acoustic branch is reduced compared to superfluid case. The gapped branche has a positive curvature at small k characteristic of the particle like nature of the excitations.

FIG. 8. The excitation spectrum of the NCSS phase ($J = 0.2U_1$, $U_2 = 0.1U_1$, $h = 1.848U_1$, $k_y = 0$). The two lower curves have been rescaled by a factor 5.

FIG. 9. At the phase boundary between the Neèl insulator and Supersolid SS the excitation spectrum vanishes as k^2 . The transition is signaled by softening of the acoustic branch proper of the supersolid ($J = 0.1U_1$, $U_2 = 0.1U_1$, $k_y = 0$).

FIG. 10. At Superfluid-Supersolid SS phase transition the roton mode vanishes as k ($J = 0.5 U_1$, $U_2 = 0.1 U_1$, $k_x = k_y$).

a)



b)

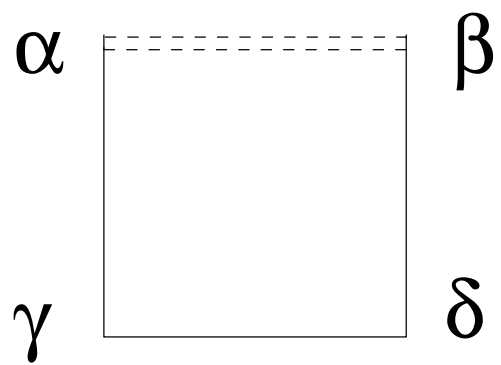
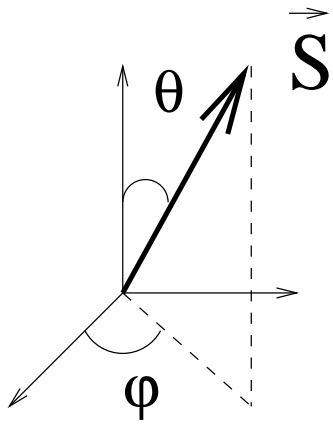
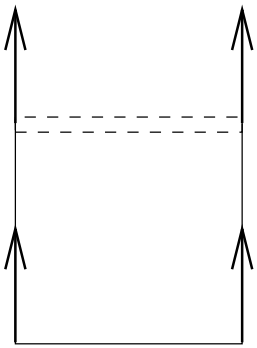


Fig.1 Amico et al.

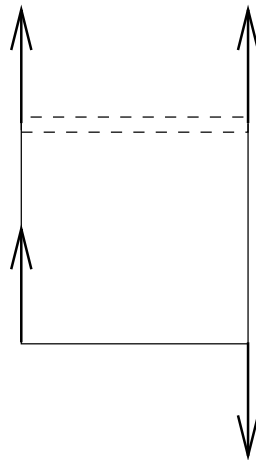
Insulating phases



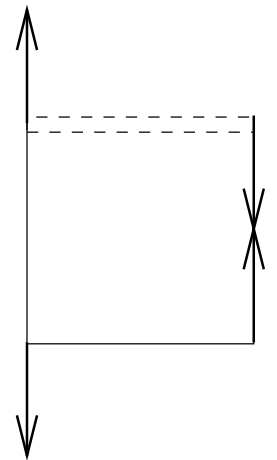
θ - configurations



integer lobe

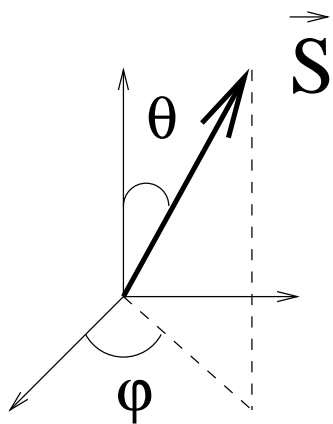


3/4 lobe



1/2 lobe

Fig2a Amico et al.



Superfluid phase

θ - configuration

ϕ - configuration

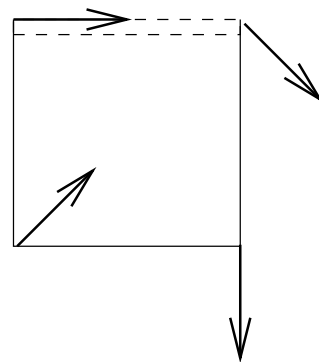
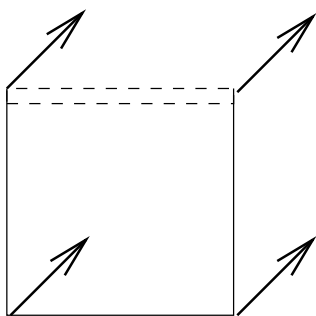
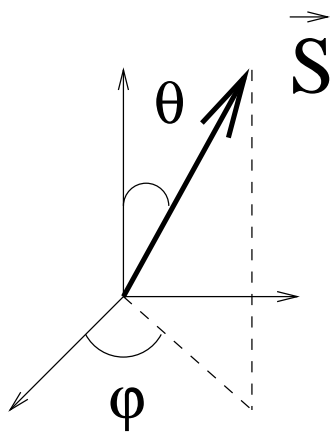


Fig.2b Amico et al.



Supersolid phase

θ - configuration

ϕ - configuration

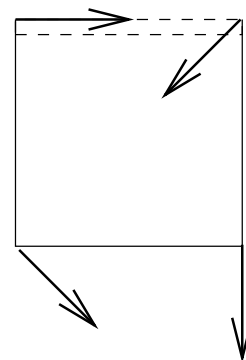
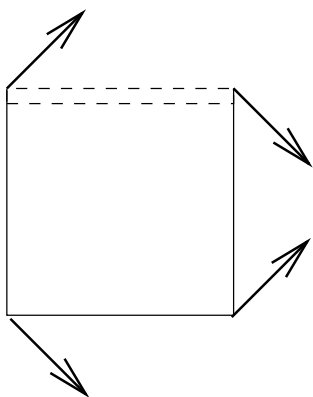
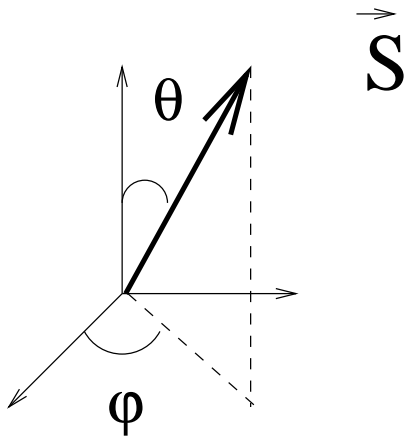


Fig.2c Amico et al.



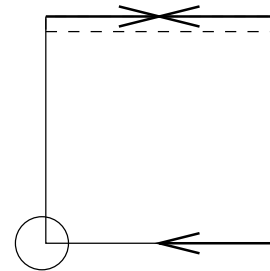
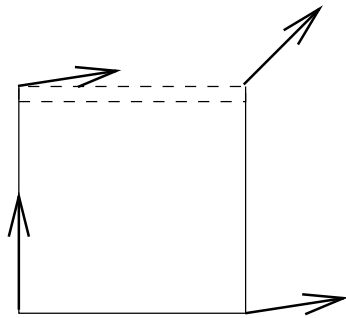
Non Chiral

Supersolid Phase

θ - configuration

ϕ - configuration

I)



II)

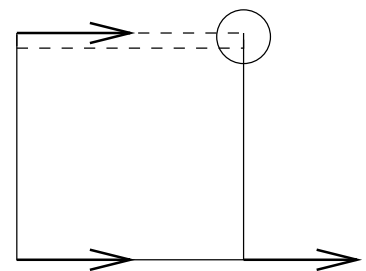
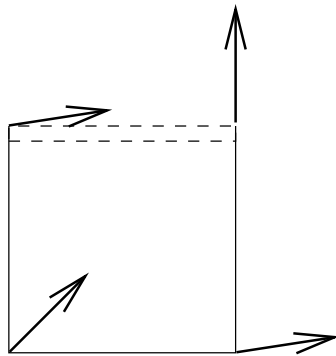
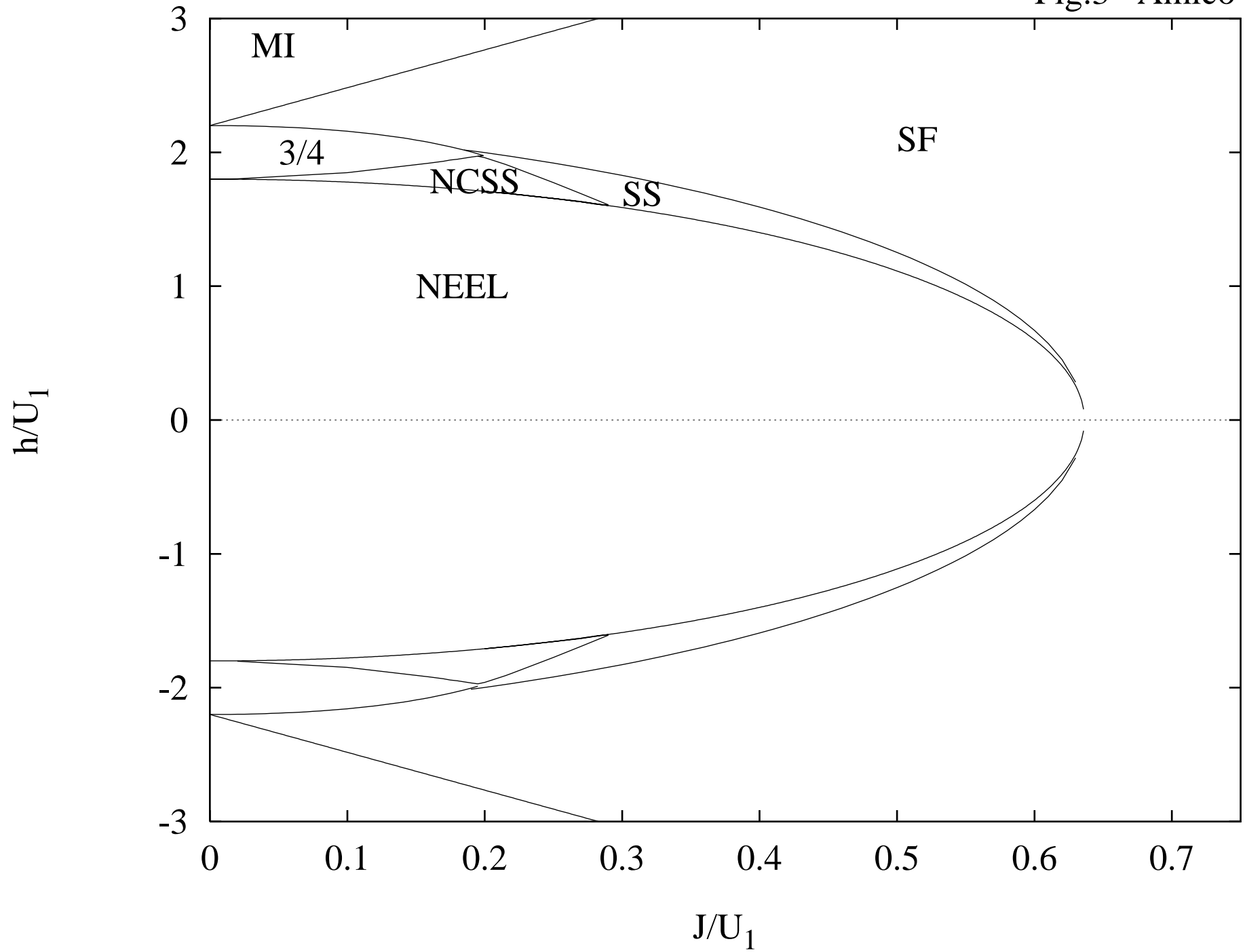


Fig.2d Amico et al.

Fig.3 Amico et al.



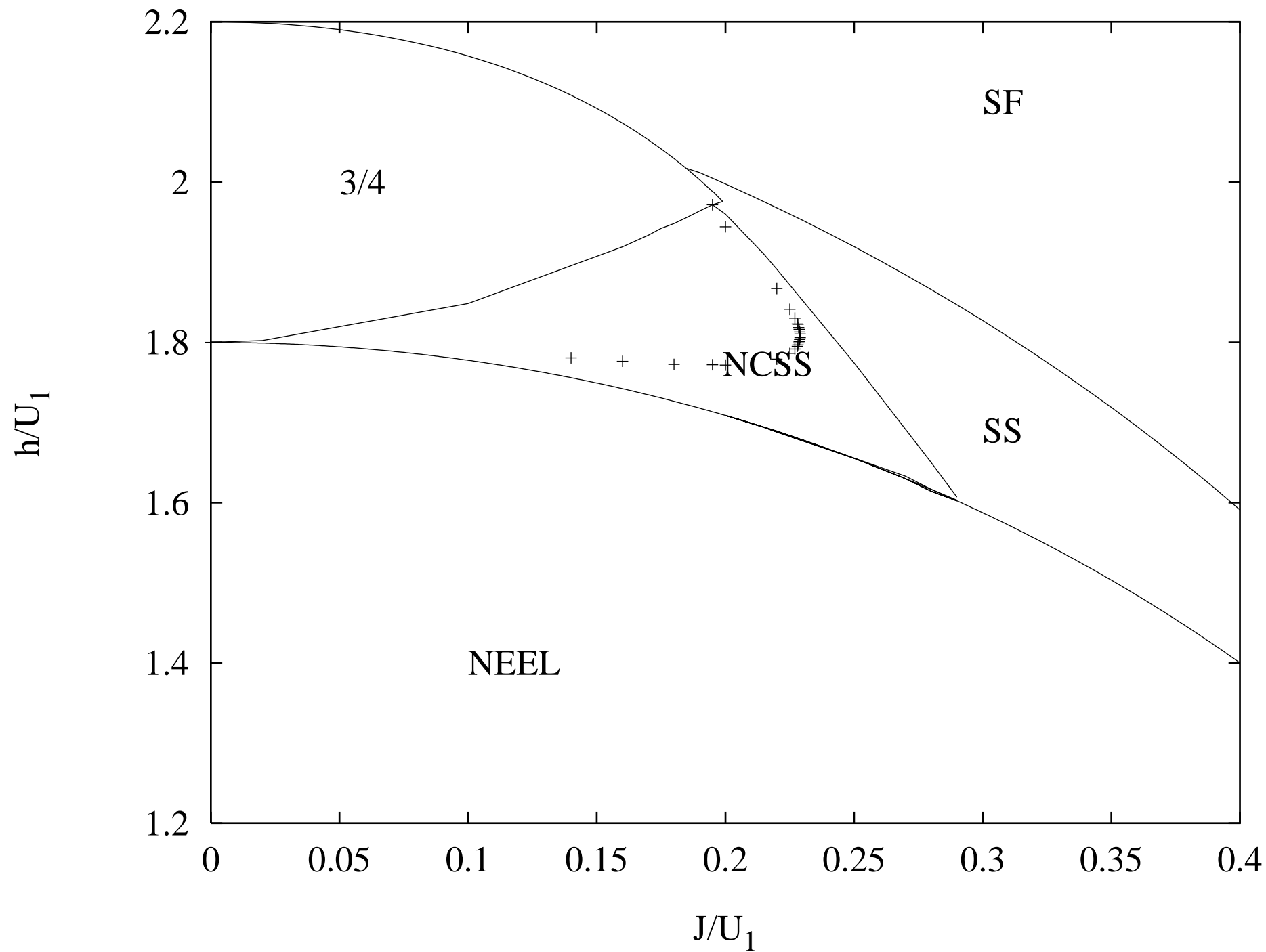


FIG.5a Amico et al.

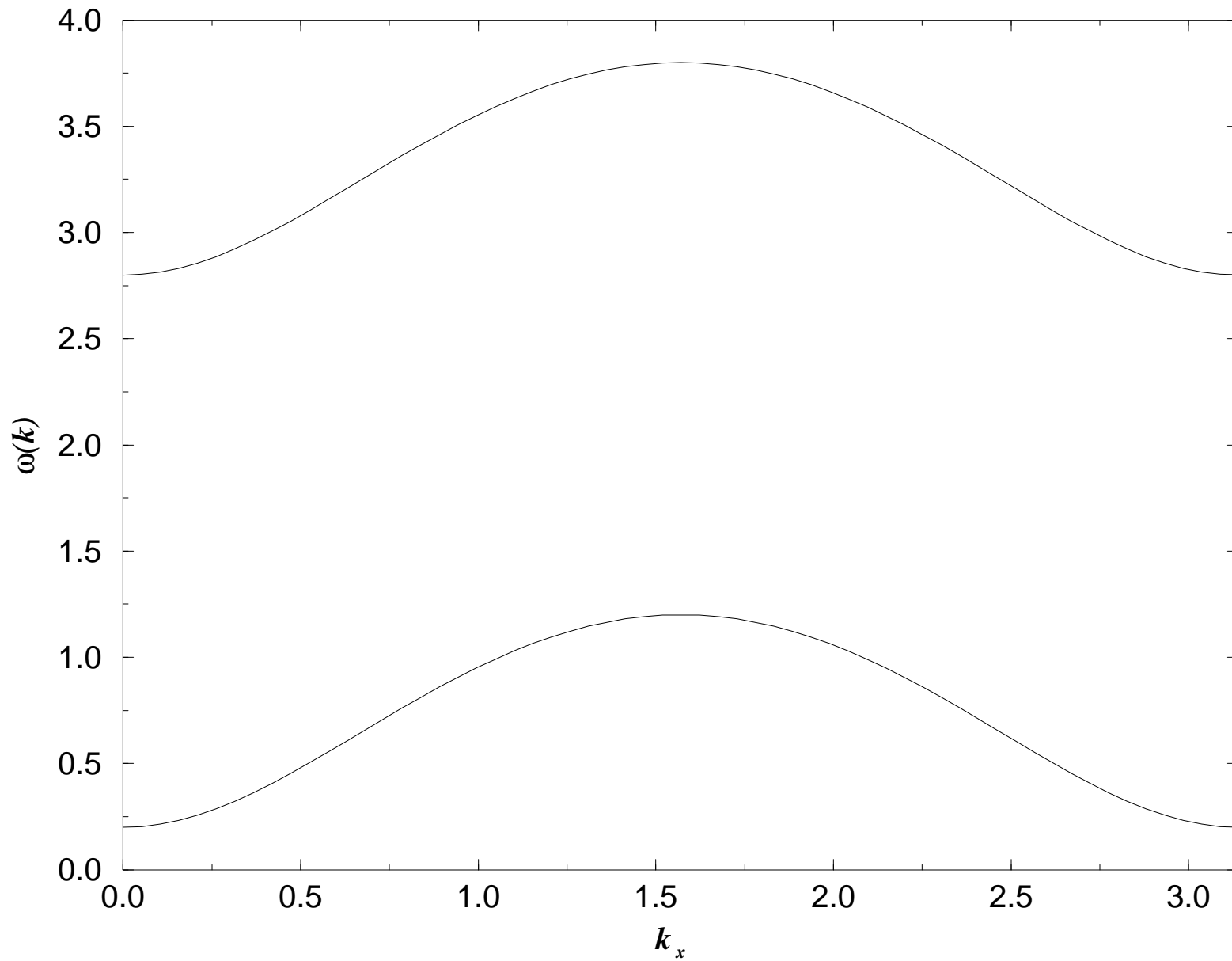


FIG.5b Amico et al.

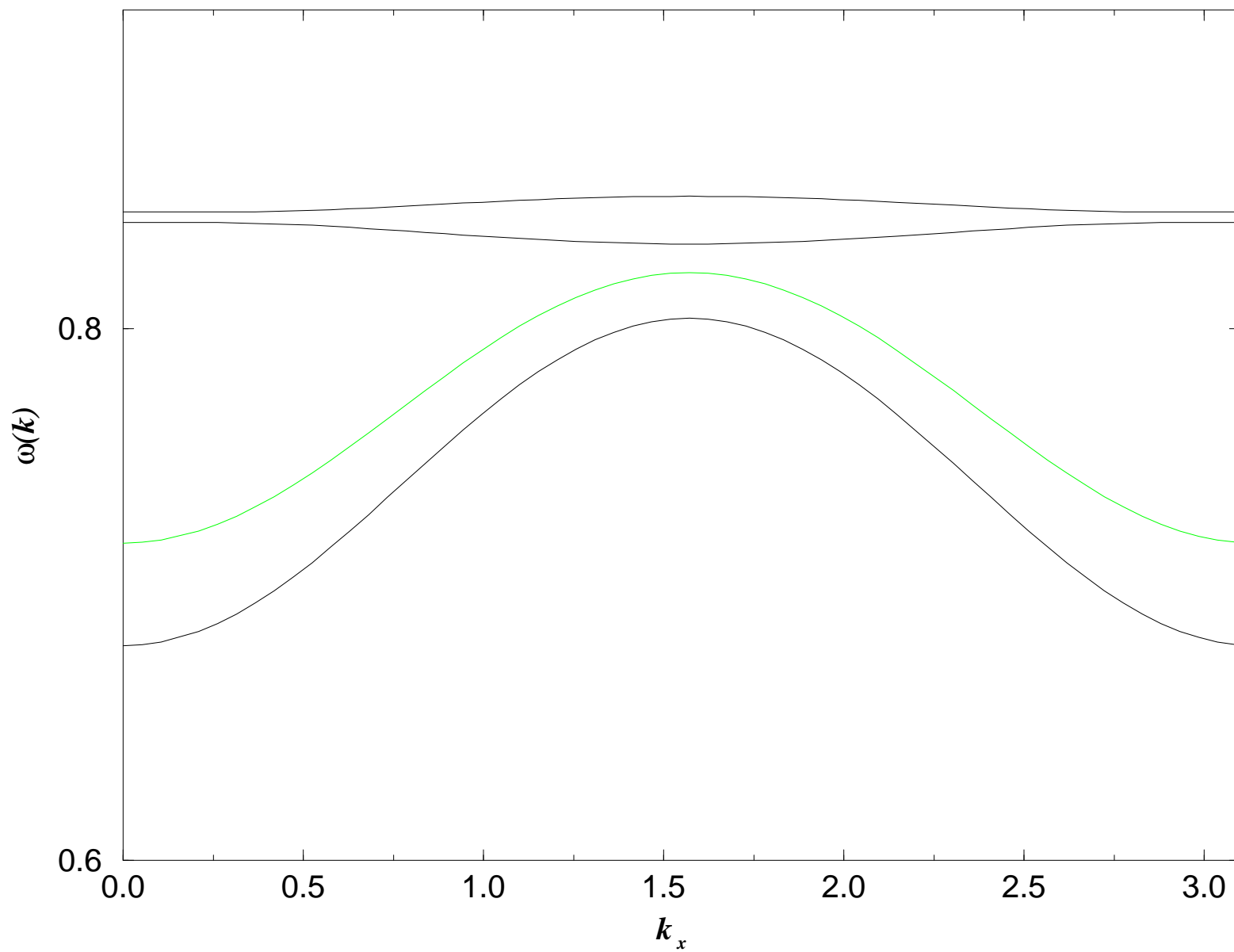


FIG.6 Amico et al.

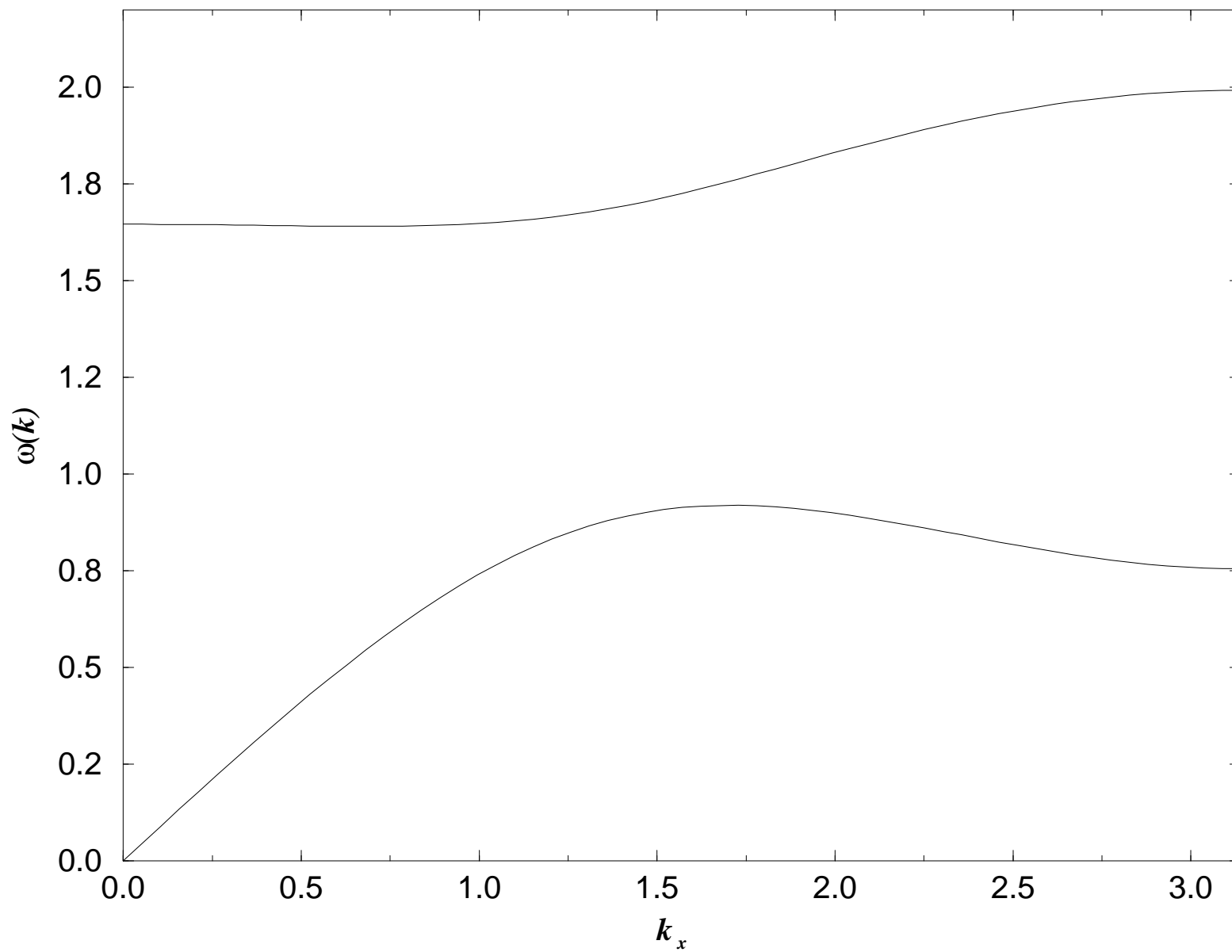


FIG.7 Amico et al.

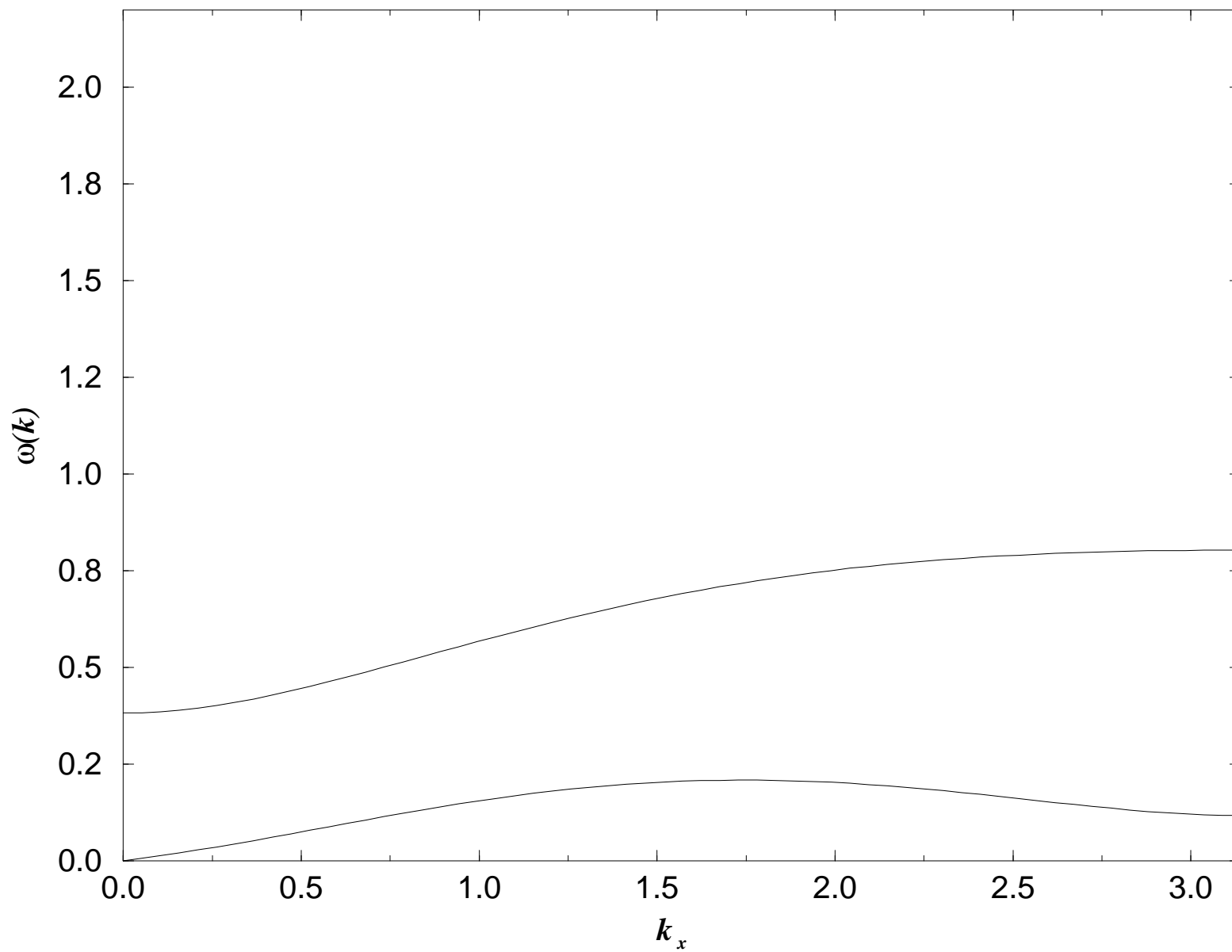


FIG.8 Amico et al.

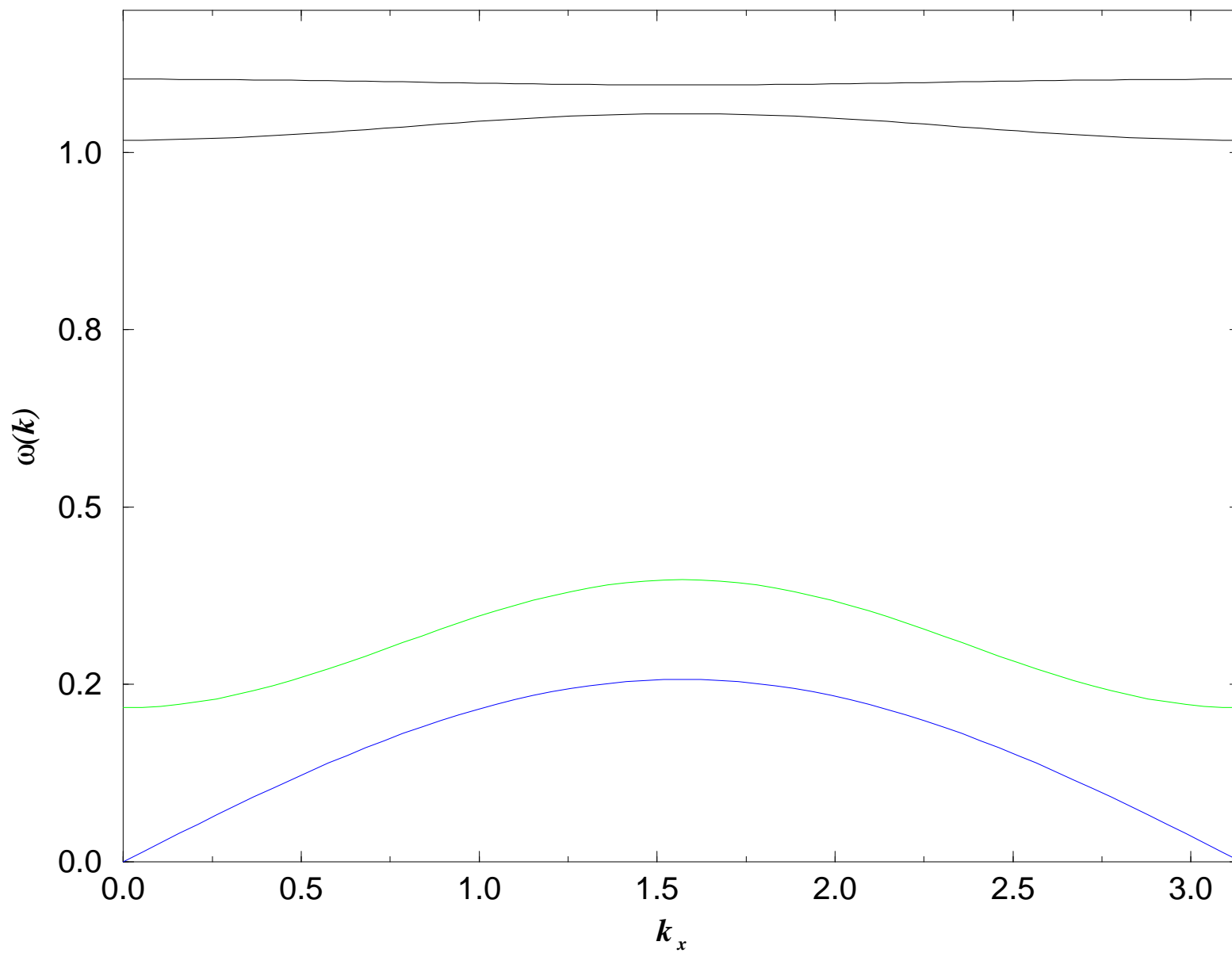


FIG.9 Amico et al.

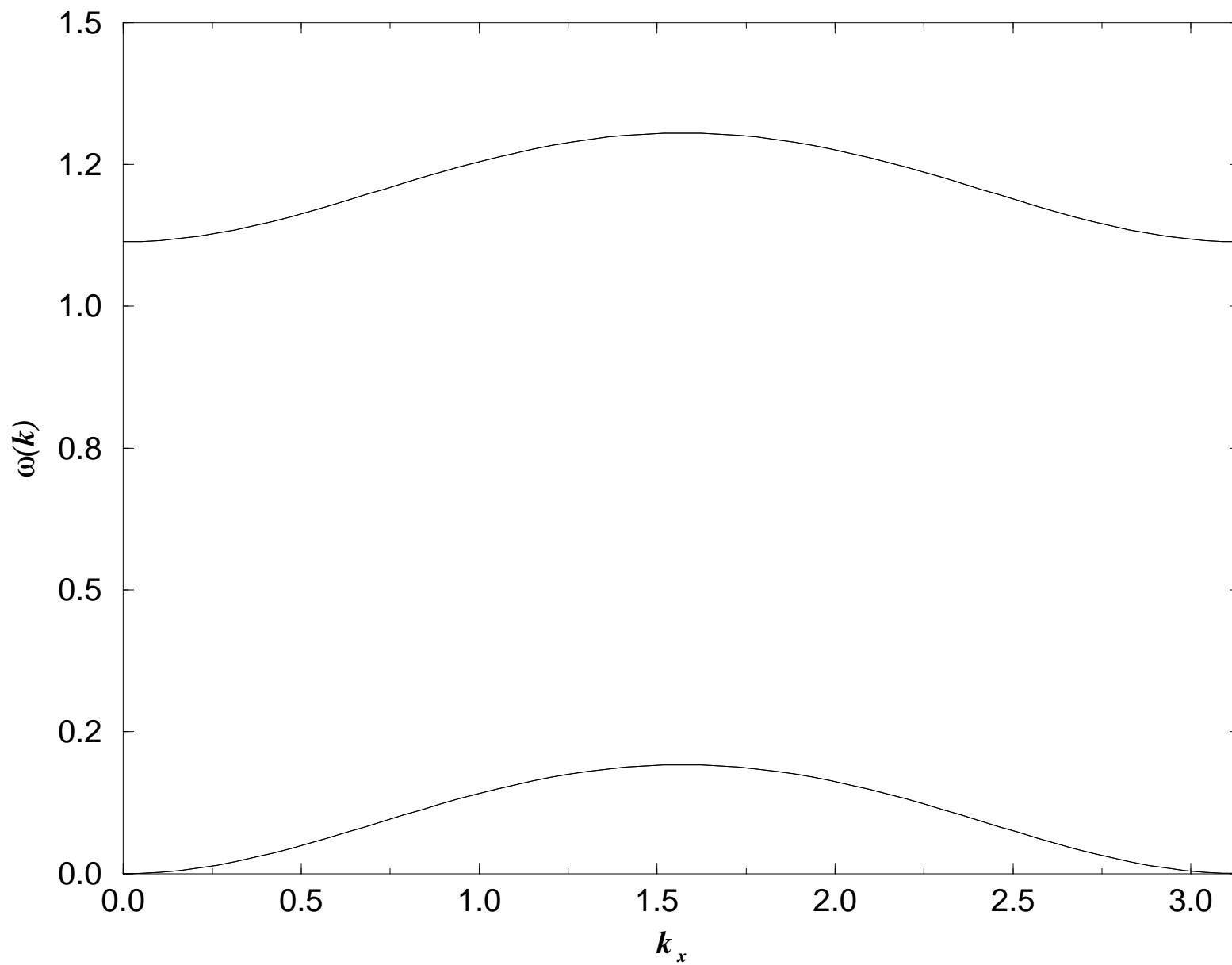


FIG.10 Amico et al.

